

Molecular Transport through a Bottleneck Driven by External Force

Chihiro NAKAJIMA and Hisao HAYAKAWA

*Yukawa Institute for Theoretical Physics,
Kyoto University, Kyoto 606-8502, Japan*

(Received July 27, 2009; Revised September 16, 2009)

The transport phenomena of Lennard-Jones molecules through a structural bottleneck driven by an external force are investigated by molecular dynamics simulations. We observe two distinct molecular flow regimes distinguished by a critical external force F_c and find scaling behaviors between external forces and flow rates. Below the threshold F_c , molecules are essentially stuck in the bottleneck due to the attractive interaction between the molecules, while above F_c , molecules can smoothly move in the pipe. A critical flow rate q_c corresponding to F_c satisfies a simple relationship with angles, and the value of q_c can be estimated from a simple argument. We further clarify the role of the temperature dependence in the molecular flows through the bottleneck.

§1. Introduction

Transport phenomena through a structural bottleneck have been widely observed and have attracted attention owing to the development of nanoscience. Many interesting bottleneck features have been observed and studied in granular flows,^{1),2)} traffic flows,^{3),4),5)} evacuation processes,^{6),7),8)} water flow through porous grains,⁹⁾ microfluidics,¹⁰⁾ Laval nozzles,¹¹⁾ and the Internet.¹²⁾ Recent technical advances have enabled us to study the nanoscale transport system such as ion transport through protein channels in a lipid membrane,^{13),14),15)} artificial nanopores,¹⁶⁾ carbon nanotubes,¹⁷⁾ Knudsen gases,^{18),19)} and domain wall motion in a wire with a notch.^{22),23),21),20)} Thus, a comprehensive understanding of transport phenomena through a bottleneck is essential.

Unlike bulk systems, the bottleneck alters the transport properties. Jamming phenomena relating the formation of a permanent arch at the bottleneck²⁴⁾ and intermittent outflows in a funnel with various angles²⁵⁾ have been observed and intensively studied.²⁶⁾ In electrical transport through quantum wires, the effect of the geometry of the wire on the transmission coefficient and conductance has been an important issue.^{27),28)} Recently, experiment and simulation studies have been performed to understand the structure and dynamics of water in a confined carbon nanotube, where it is discussed that confinements induce the phase transition not observed in a bulk system.^{29),30)} In the transport phenomena through the bottleneck, these collimator effects such as the curvatures and cross sections of the passage play a crucial role in the transport phenomena. In such situations, a useful approach to treat transport phenomena through a bottleneck is computer simulations. Various simulation techniques, such as driven lattice gases,^{31),32)} cellular automata,³³⁾ and molecular dynamics (MD)³⁴⁾ have been designed and applied to probe these trans-

port mechanisms. Numerically, the existence of scaling behavior of escape dynamics through a bottleneck^{35),36)} and the power spectra of the flow in an hourglass³⁷⁾ have been investigated.

In this paper, we address the problem of the steady particle flow in a pinched pipe under an external force. We restrict our attention to a highly simplified two-dimensional model, considering geometric effects in the hope to gain some generic physical insight. We intend to evaluate the importance of the curvature of the pipe, particle area fractions, and external forces. This goal may be achieved through detailed simulations of the motion of particles. For these reasons, we perform MD simulations to investigate molecular flows in the pipe with various angles.

The present article is organized as follows. In §2, we discuss the model and MD simulation techniques. In §3, the results of the MD simulation and data analyses are presented. Special emphasis is placed on the relationship between stationary molecular flows and external forces at various angles and scaling behavior of these relations. Then, we demonstrate that flow rates against angles give a simple relation and estimate the value of the critical flow rate. We investigate the fluctuation of the flow and the fundamental diagram for molecular flows in analogy to a traffic model. We further investigate the temperature dependence of the molecular flow and how flow rates depend on the ratio between molecular size and pipe width. For comparison, we observe a molecular flow that has only repulsive interactions. We conclude and discuss our results in §4.

§2. Model

Let us consider a two-dimensional symmetric pipe shown in Fig. 1(a). The pipe has symmetry configuration, like an hour glass, and is represented by the hyperbolic tangent $y = 36 \tanh(x \tan \theta / 36)$ with the angle θ defined by the slope of hyperbolic tangent.

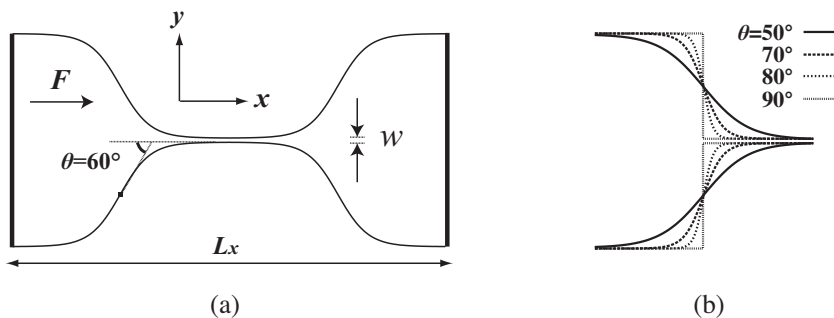


Fig. 1. (a) Schematic of a two-dimensional symmetric pipe with angle θ , which is characterized by the slope of $y = 36 \tanh(x \tan \theta / 36)$. The x -directional pipe length is $Lx = 300\sigma$ and the narrowest pipe width is w . The wall is constructed of particles that are attached to other particles by a linear spring, and the y -directional boundary is the thermal wall with temperature $T = 0.1\epsilon$. (b) Schematic of left region of the pipe with angle $\theta = 50^\circ, 70^\circ, 80^\circ, 90^\circ$.

The molecules are interacting via Lennard-Jones (LJ) potential:

$$\phi_{\text{LJ}}(r_{ij}) = 4\varepsilon \left\{ \left(\frac{\sigma}{r_{ij}} \right)^{12} - \left(\frac{\sigma}{r_{ij}} \right)^6 \right\}, \quad (2.1)$$

where ε is the energy scale of the interaction, σ is the diameter of each molecule, and r_{ij} is the separation between particles i and j . The pair interactions are truncated at $r_{ij} = 3\sigma$ for numerical convergences. The linear x -directional pipe length is $L_x = 300\sigma$. In most of our simulations, the narrowest pipe width w is 3σ , but we will later investigate the width dependences on the flow rate. The wall is composed of molecules that are attached to other molecules by linear springs with spring constant $\kappa = 20000\varepsilon/\sigma^2$, but the molecules at both edges are fixed. The wall molecules are interacting with driven molecules via the same LJ potential. In the presence of the x -directional external force F , the current of the molecules will be maintained, and hence, the system will always remain in a nonequilibrium stationary state.

In the horizontal boundaries, we adopt the periodic boundary conditions for the positions of molecules and the thermal walls for the velocity of molecules, which give the random velocity whose probability distribution function is given by

$$f(\mathbf{v}) = \frac{1}{\sqrt{2\pi}} \left(\frac{m}{k_B T} \right)^{3/2} |v_x| e^{-\frac{mv^2}{2k_B T}} \quad (2.2)$$

with temperature $T = 0.1\varepsilon$. Owing to the presence of the x -directional external forces, molecules keep flowing from left to right through the bottleneck.

For comparisons of LJ molecular flows, we adopt the purely repulsive Weeks-Chandler-Andersen (WCA) potential given by

$$\phi_{\text{WCA}}(r_{ij}) = \begin{cases} 4\varepsilon \left\{ \left(\frac{\sigma}{r_{ij}} \right)^{12} - \left(\frac{\sigma}{r_{ij}} \right)^6 + \frac{1}{4} \right\} & , (x \leq 2^{1/6}\sigma) \\ 0 & , \text{otherwise} \end{cases} \quad (2.3)$$

which we call WCA for later discussion.

MD simulation is carried out for the dynamics of the molecules under the different geometrical pipes. The equation of motion is solved by using the velocity-Verlet method with a time step $\Delta t = 0.001\tau$, where $\tau = \sigma(m/\varepsilon)^{1/2}$. The mass of the driven molecule is m and that of the wall is $10m$ to avoid the change in the pipe configuration due to the molecular flow through the pipe. The initial positions of molecules are arranged not to contact each other, and the initial velocities of the molecules are given by the Maxwell distribution with temperature $T = 0.1\varepsilon$. In our reduced units, the unit length σ , unit energy ε , molecular mass m , and Boltzmann constant k_B are set equal to unity. As shown in Fig. 1(b), we vary the pipe angle $\theta = 50^\circ, 55^\circ, 60^\circ, 65^\circ, 70^\circ, 75^\circ, 80^\circ, 85^\circ, 90^\circ$. As the angles become large, each pipe represents a narrow straight passage with a narrowed entrance and constant pipe width, whereas the pipe with a small angle exhibits a pinched configuration. The pipe configuration less than angle $\theta = 50^\circ$ is not used since the y -directional pipe length becomes markedly short in our model.

To investigate molecular flows in the pinched pipe, we mainly measure the flow rate q in the pipe with various angles, which is the numbers of crossing-driven molecules during the time at the middle cross section. In the steady flow, the flow rate q should be a constant in any cross section owing to the continuity equation in the stationary state. After $t = 1.5 \times 10^4 \tau$, we collect the statistical quantities as the system reaches a steady state.

§3. Steady molecular flow

3.1. Steady molecular flow at various angles

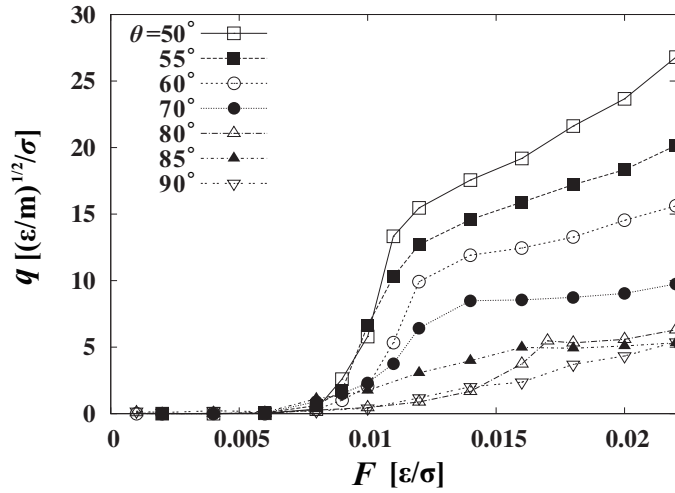


Fig. 2. Plots of the flow rates q against the various external forces F in the pipe with angle $\theta = 50^\circ$, 55° , 60° , 70° , 80° , 85° , 90° .

We study steady molecular flows through the pipes with various angles. The narrowest width of each pipe is three times the molecule diameter. The driven molecule number in the pipe is $N = 3510$. Figure 2 plots the flow rate q against the external force F under various angles. In the case of small external forces, driven molecules jam in the pipe and stick on the wall since the molecular interactions are sufficiently strong compared with external forces, while as the external forces increase, the nonlinear flow growth is observed and jamming is insignificant owing to the dominance of the external forces. These transport phenomena are clearly observed in the pipes with angle below $\theta = 80^\circ$. On the other hand, as Fig. 3 shows, the distinct relation between the flow rate and external force is difficult to observe at the angle above $\theta = 80^\circ$ owing to the small amount of molecular flow caused by the markedly narrow pipe entrance and the passage at these angles. At angle $\theta = 90^\circ$, the molecular arch is observed in the low external force. Figure 4 exhibits the existence of a molecular arch in the entrance of the pipe with angle $\theta = 90^\circ$ under the external force $F = 0.010\epsilon/\sigma$. This phenomenon could be caused by the straight corner at the pipe entrance.

To investigate the molecular flow properties further, we perform the semilog plot

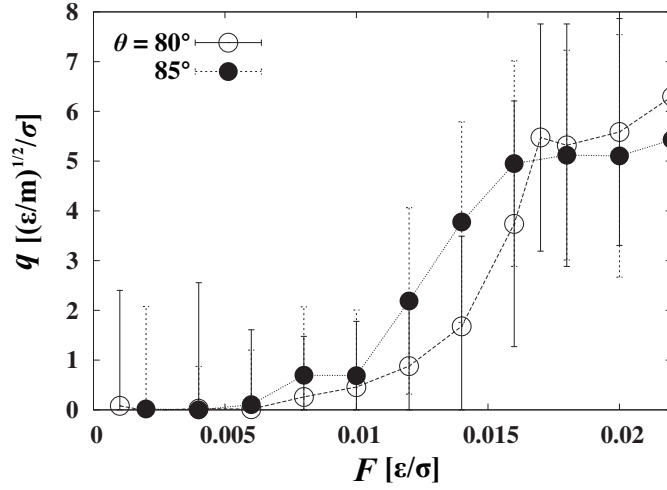


Fig. 3. Plots show the flow rates q against the external forces F at the angle $\theta = 80^\circ$ and 85° with variance.



Fig. 4. A schematic pipe graph at the angle $\theta = 90^\circ$ and the external force $F = 0.010\epsilon/\sigma$. The entrance of the pipe exhibits arch formation.

of the flow rate, $\log q$, against the external force F . The inset of Fig. 5 indicates the existence of two distinct molecular flow regimes in the pipe with angle $\theta = 60^\circ$. The flow rate and external force at the crossover of these regimes, q_c and F_c , are considered to correspond to the balance of external forces and molecular interactions. These transport phenomena are observed at the angle below $\theta = 80^\circ$ and q_c and F_c are determined at each angle. At the angle above $\theta = 80^\circ$, it is difficult to distinguish characteristic crossover from the relation between flow rates and external forces. By using q_c and F_c in each pipe, the scaled flow q/q_c against the scaled external force F/F_c can be plotted in Fig. 5. The solid and dotted lines are fitted by curves $q/q_c = \exp(aF/F_c - b)$ with $a, b = (8.45, 8.48)$ for molecular flow below F_c and $(0.445, 0.431)$ for molecular flow above F_c , respectively. Thus, it is shown that flow rates as a function of external forces are given by the two distinct simple exponential forms and are independent of the pipe geometry in these regimes.

The angle dependences on q_c can be simply studied. Figure 6 is the plot of q_c as a function of the angle. At a large angle, pipe configurations represent the

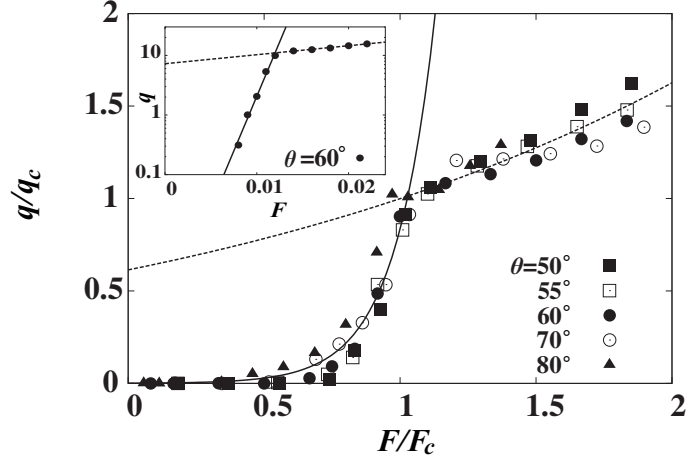


Fig. 5. Plot of the scaled flow q/q_c against the scaled external force F/F_c at the angle $\theta = 50^\circ, 55^\circ, 60^\circ, 70^\circ, 80^\circ$. The solid line is fitting curve $q/q_c = \exp(aF/F_c - b)$ with $a, b = (8.45, 8.48)$ for molecular flow below F_c and the dotted line is $a, b = (0.445, 0.431)$ for molecular flow above F_c . The inset shows a semilog plot of the flow rate and the external force in the pipe with angle $\theta = 60^\circ$. We define the crossover of two flow lines as F_c and q_c .

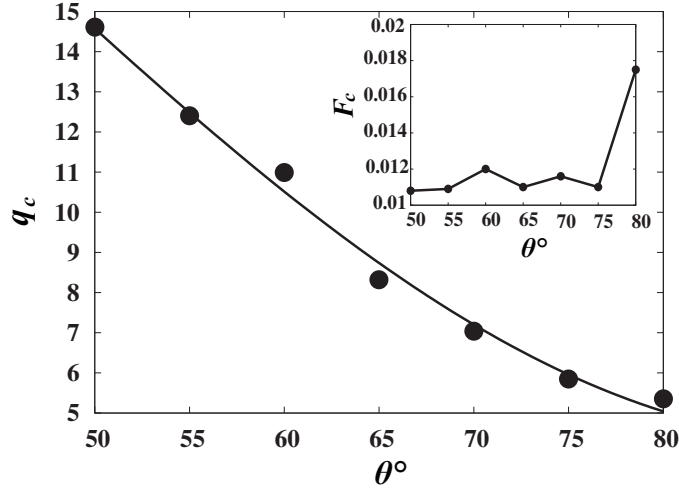


Fig. 6. Critical flow rate q_c as a function of the pipe angle θ . The solid line is the fitted curve $\alpha \cos^2 \theta + q_0$ with $\alpha = 25.9(\varepsilon/m)^{1/2}/\sigma$ and $q_0 = 4.21(\varepsilon/m)^{1/2}/\sigma$. The unit of the vertical axis is $(\varepsilon/m)^{1/2}/\sigma$. The inset shows the plot of the critical external force F_c [ε/σ] against the angle θ .

reduced passage so that it is plausible for the molecular flow to decrease against the angles. We are aiming at a rough theoretical estimation of variations of q_c against the angles. In the presence of F_c , the system is considered to be balanced between the external force and the molecular interaction. We assume that the practical external force along the pipe with angle θ , $F_c \cos \theta$, drives molecules in the pipe. This practical external force is set off in the y -direction owing to the symmetric pipe configuration; thus, the x -component of the practical external force $\tilde{F} \simeq F_c \cos^2 \theta$

could be dominant for molecular flows. Since we consider the steady state, the particle density in the filled pipe region $\bar{\rho}$ and the terminal velocity $v \simeq \mu \tilde{F}$ with the mobility μ are considered to be constant. Thus, the flow rate at the balanced point is approximated by

$$q_c \simeq \alpha \cos^2 \theta + q_0, \quad (3.1)$$

with fitting parameters α and q_0 , where q_0 is the extrapolation of the critical flow rate at $\theta = 90^\circ$. In Fig. 6, the solid line represents (3.1) with $\alpha = 25.9(\varepsilon/m)^{1/2}/\sigma$ and $q_0 = 4.21(\varepsilon/m)^{1/2}/\sigma$ and is well fitted at the angle below $\theta = 80^\circ$. On the other hand, the relation F_c and the angle are almost independent of the angle under $\theta \leq 75^\circ$ in the inset of Fig. 6. At the angle above $\theta = 80^\circ$, the value of F_c that corresponds to the value of q_c cannot be determined since the crossover is not clearly observed.

We further estimate the value of q_c , which corresponds to F_c . The critical flow rate q_c is given by

$$q_c = n v_c S, \quad (3.2)$$

where $n = 4\phi/(\pi\sigma^2)$ is the number density with the area fraction ϕ , v_c is the critical velocity, and S is the cross section. The critical velocity is represented by the escape velocity from the bottom of LJ potential as $v_c = \sqrt{2|\phi_{LJ}(a)|/m}$ with the distance at the minimum potential $a = 2^{1/6}\sigma$. Thus, the critical flow rate can be estimated by

$$q_c = \frac{12\sqrt{2}}{\pi} \frac{1}{\sqrt{m\sigma}} \phi. \quad (3.3)$$

The area fraction at the region where the particles accumulate is $\phi \simeq 0.7$ in our model, so that we can estimate the value of the critical flow rate as $q_c \simeq 3.8\sqrt{\varepsilon/m}/\sigma$. This value is close to the critical flow rate q_0 at the angle $\theta = 90^\circ$. Thus, these theoretical estimations are plausible for the explanation of our molecular transport.

3.2. Fluctuation of the flow

We next investigate how the fluctuation of the flow depends on the external force. To clarify the characteristics of the fluctuation, we introduce the normalized standard deviation σ^* obtained by the linear interpolation of the standard deviations $\sigma[q_1/q_c]$ and $\sigma[q_2/q_c]$, where q_1 and q_2 are the closest points from q_c ($q_1 \leq q_c \leq q_2$). Figure 7 shows the standard deviation of the scaled flow rate $\sigma[q/q_c]/\sigma^*$ against the scaled external force F/F_c at the angle $\theta = 50^\circ, 55^\circ, 60^\circ, 65^\circ, 70^\circ, 80^\circ$. As Fig. 7 shows, the scaled standard deviation $\sigma[q/q_c]/\sigma^*$ increases gradually below the external force $F < F_c$, where the particles are essentially stuck in the bottleneck and the fluctuations are suppressed. For the large external forces $F > F_c$ the scaled standard deviation is almost constant in any pipe angle and the fluctuation of the flow is insensitive to the external force. These fluctuation phenomena almost correspond to Fig. 5 (the relation between the scaled flow rate and the scaled external force). It is interesting that the fluctuation of the flow does not have any specific peak around F_c , and the critical fluctuation continues above $F > F_c$, while we do not make clear its reason.

Furthermore, we investigate how the fluctuation depends on the angle. Figure. 8 shows the standard deviation of the flow $\sigma[q]$ against the angle θ at the constant external forces $F = 0.020, 0.016, 0.004\epsilon/\sigma$, and the inset of Fig. 8 shows the corresponding flow rate q against the angle θ . In each external force, the standard deviation of the flow rate is substantially constant and does not exhibit any fluctuation peak against the angle. Although we have investigated the relation between the fluctuation and the angle, the angle dependence of the fluctuation of the flow is not observed in our model.

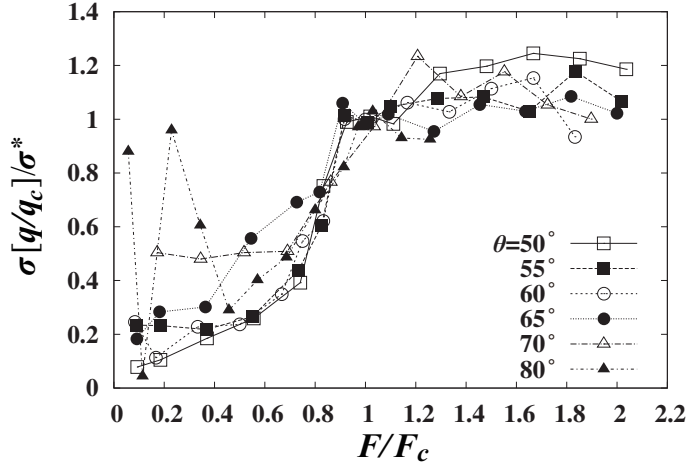


Fig. 7. Standard deviation of the scaled flow rate $\sigma[q/q_c]/\sigma^*$ against the scaled external force F/F_c at the angle $\theta = 50^\circ, 55^\circ, 60^\circ, 65^\circ, 70^\circ, 80^\circ$. The normalized standard deviation σ^* is the linear interpolation of the standard deviations $\sigma[q_1/q_c]$ and $\sigma[q_2/q_c]$, where q_1 and q_2 are the closest points from q_c ($q_1 \leq q_c \leq q_2$) in each angle.

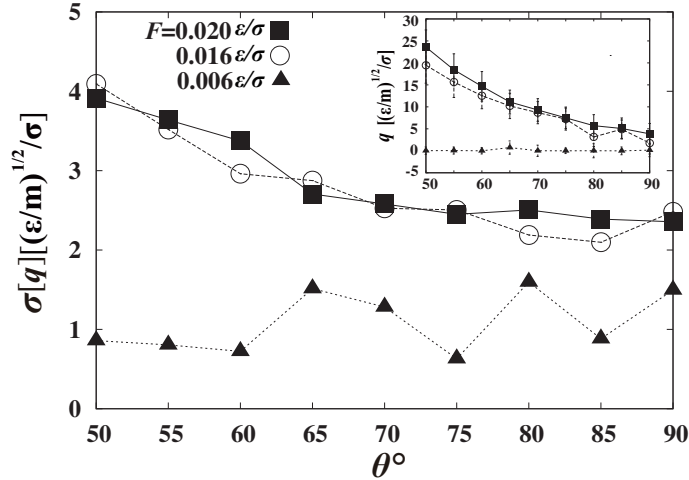


Fig. 8. Standard deviation of the flow rate $\sigma[q]$ against the angle θ in the external force $F = 0.020, 0.016, 0.006\epsilon/\sigma$. The inset shows the corresponding flow rate q against the angle θ .

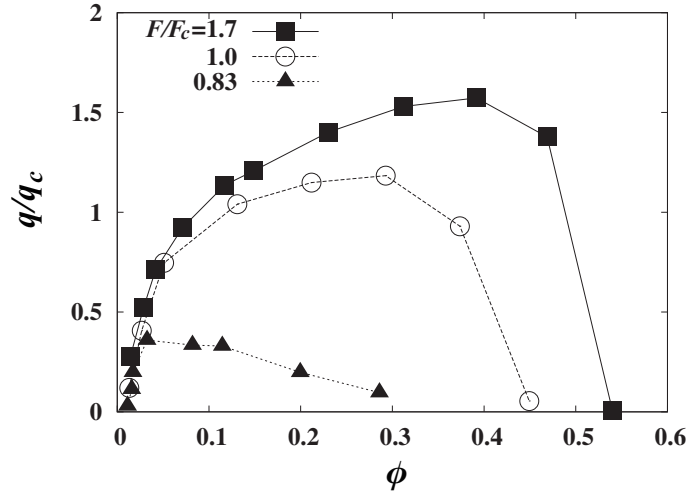


Fig. 9. Scaled flow rate q/q_c as a function of the area fraction $\phi[1/\sigma^2]$ under scaled constant external forces $F/F_c = 0.83, 1.0, 1.7$ with $F_c = 0.012\varepsilon/\sigma$.

3.3. Fundamental diagram

For traffic flows, the functional relations between vehicle currents and vehicle densities have attracted much attention, which is called the fundamental diagram.³⁾ In our model, we investigate the relation between the molecular flow rate and the molecular area fraction under constant external forces. We define the area fraction ϕ as the average area fraction in upstream regions ($0 < x < 150\sigma$), which corresponds to the accumulated molecular height from the middle of the pipe. Figure 9 shows the scaled flow rate q/q_c as a function of ϕ in the pipe with angle $\theta = 60^\circ$ and the narrowest pipe width 3σ . In each scaled external forces F/F_c , scaled flow rates exhibit the linear dependence of ϕ in low area fractions, while scaled flow rates decrease in high area fractions. These behaviors in our system are independent of F_c and similar to traffic flow behaviors.

The existence of the metastable branch is often discussed in the fundamental diagram of the traffic flow, while the present model does not exhibit such behaviors. As the previous subsection has shown, we cannot observe any fluctuation peak of the flow in both Figs. 7 and 8. These results likely relate the lack of the metastable branch in our model. Thus, the flow rate may be represented by a single curve in our fundamental diagram.

3.4. Width dependence of flow rate

In the situation of gravity-driven granular flow, jamming transitions depend on the ratio between the exit size and the grain size.²⁴⁾ Thus, we investigate the relation between flow rates and pipe widths under constant external forces. We fix a pipe configuration with the angle $\theta = 60^\circ$, but vary the pipe width of the narrowest part from $w = 1.5\sigma$ to $w = 6\sigma$. The driven particle number is $N = 3510$ and the external force is $F = 0.012\varepsilon/\sigma$, which is above F_c and $F = 0.008\varepsilon/\sigma$ below F_c . Figure 10 shows the flow rate q against the narrowest pipe width w . In $F = 0.012\varepsilon/\sigma$, no

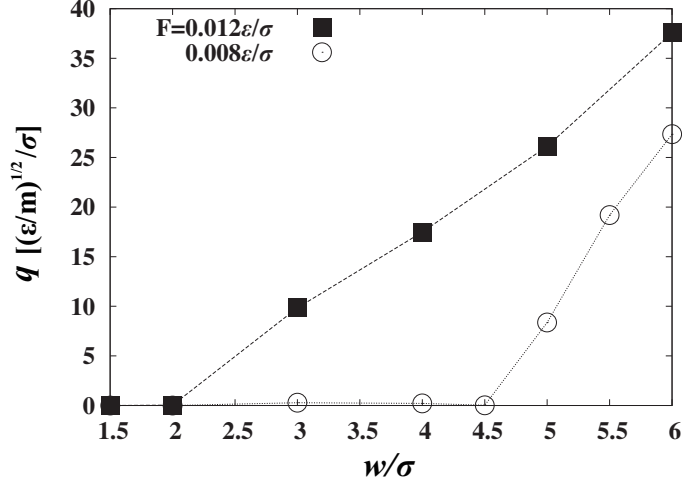


Fig. 10. Flow rate q as a function of the pipe width at the angle $\theta = 60^\circ$ and external force $F = 0.012\epsilon/\sigma$ and $0.008\epsilon/\sigma$. Dotted lines are connected data.

molecular flow is observed in the pipe width under $w = 2\sigma$, which is too narrow to pass through molecules. In $F = 0.008\epsilon/\sigma$, we observe no molecular flow below $w = 4.5\sigma$ owing to the low external forces. On the other hand, there exists the flow when the width is larger than $w = 2\sigma$ for $F = 0.012\epsilon/\sigma$ and $w = 4.5\sigma$ for $F = 0.008\epsilon/\sigma$. Although the proportional constant depends on the external force, we observe that q is almost proportional to the cross section of the pipe in this flow region.

3.5. Temperature dependence

To investigate the temperature dependence on the flow rate, we consider LJ molecule at the temperature $T = 0.1, 0.2, 0.3, 0.4\epsilon$ in the pipe with the angle $\theta = 60^\circ$ and the width 3σ and molecular number $N = 3510$. Figure 11 shows the scaled flow rate q/q_F , where q_F is the flow rate at the external force $F = 0.020\epsilon/\sigma$, as a function of the external forces. As we have shown in Fig. 5, there is the “jammed region” for $F < F_c$ at the temperature $T = 0.1\epsilon$. However, as the temperature becomes large, LJ molecules can flow smoothly in the “jammed” region ($F < F_c$) and the flow rate increases linearly against the external force. It is known that $T \cong 0.5\epsilon$ is the transition temperature from the gas phase to the liquid phase for the wide range of the density.³⁸⁾ As Fig. 11 shows, we can observe the smooth flow at the temperature $T \gtrsim 0.4\epsilon$, so that this “jamming” phenomena likely relate gas-liquid phase transition. At the low temperature $T = 0.1\epsilon$, LJ molecules are regarded as in liquid phase, so that the correlated motion of the liquid molecule may cause no molecular flow and dominate the “jamming” phenomena in the pipe.

We also investigate the temperature dependence on the flow in the constant external forces. Figure 12 shows the flow rate q with the standard deviation as a function of temperature T in the external field $F = 0.004\epsilon/\sigma$ and $0.012\epsilon/\sigma$. In the case of the external force $F = 0.004\epsilon/\sigma$, LJ molecules are almost stuck at the

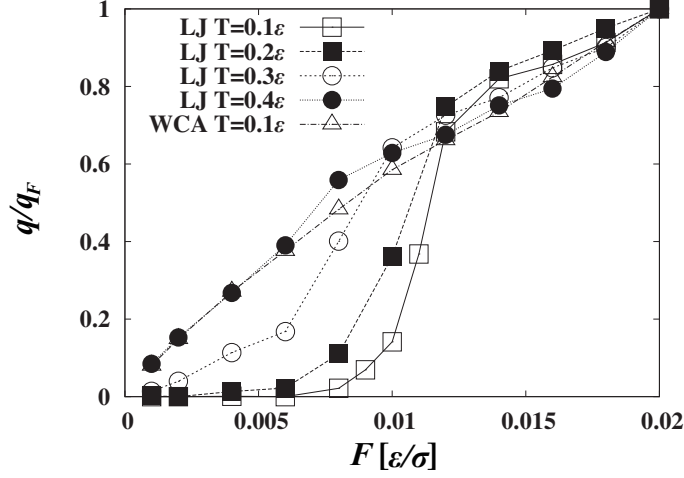


Fig. 11. Scaled flow rate q/q_F as a function of the external force in the pipe with angle $\theta = 60^\circ$, where q_F is the flow rate at $F = 0.020\epsilon/\sigma$, for LJ molecule at the temperature $T = 0.1, 0.2, 0.3, 0.4\epsilon$ and WCA molecule at the temperature $T = 0.1\epsilon$.

low temperature and begin to flow above about $T = 0.2\epsilon$. In the case of the large external force $F = 0.012\epsilon/\sigma$, LJ molecules flow even in the low temperature and the “jamming” phenomena do not happen. At high temperature, “jamming” phenomena do not occur and, in addition, we have observed that “jamming” phenomena depend on the external force.

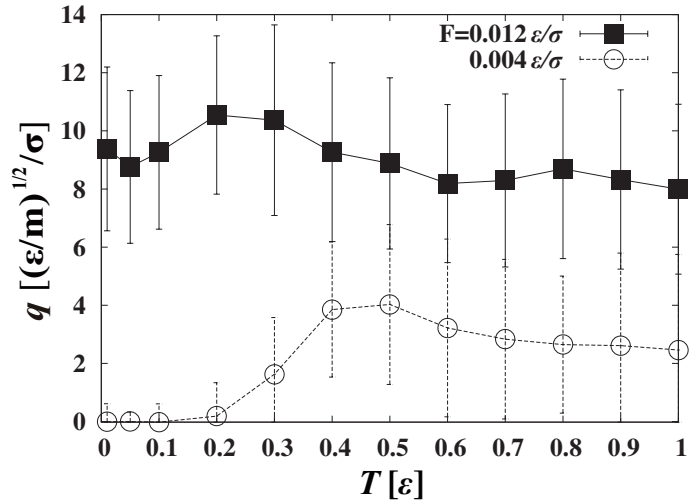


Fig. 12. Flow rate q with the standard deviation as a function of the temperature T at the external field $F = 0.004\epsilon/\sigma$ and $0.012\epsilon/\sigma$ in the pipe with angle $\theta = 60^\circ$.

3.6. WCA potential

Thus far, we have investigated the transport of LJ molecules that have both attractive and repulsive interactions against other molecules. To extract the role of attractive interactions, we study the molecular flow with WCA potential ϕ_{WCA} in eq. (2.3). As the same condition of LJ molecular flow, the angle $\theta = 60^\circ$, the width 3σ , and molecular number $N = 3510$ are used. The plot of the triangle in Fig. 11 shows WCA molecule flow. LJ molecular flow at the temperature $T = 0.1\varepsilon$ is represented by two exponential functions as mentioned earlier, while WCA molecular flow can be fitted using a single exponential function. In the large external forces, LJ and WCA molecular flows exhibit an identical behavior, since external force is dominant for both flows.

Furthermore, we investigate whether the arch effect appears for the WCA model at the pipe with the angle $\theta = 90^\circ$. The WCA molecule can flow smoothly in the pipe in any external force and even at low temperature, so that we observe no arch effect for the WCA model. These results indicate that the attractive force and low temperature are dominant for "jamming" phenomena.

§4. Discussion and conclusions

We have studied the molecular transport through bottlenecks, which is inspired by nanoscale transport phenomena such as biological ion transport. In this study, we simplify the bottleneck as the two-dimensional pinched pipe characterized by the angle θ and width w . As the external forces increase, we can observe two distinct molecular flow regimes. Using the value at the crossover of these regimes, which is considered to correspond to the balance of the molecular interaction and the external force, the scaling behaviors of the flow rate and external force are observed in our model. These scaling behaviors show that the flow rate does not depend on the pipe configurations at the angle below $\theta = 80^\circ$. However, at the large angle, we cannot clarify the relation between the flow rate and external force owing to the small amount of molecular flow. The flow rate as a function of the angle is also observed, and this relation is verified using a simple theory. We further exhibit the value of the critical flow rate from rough theoretical estimations. These double exponential forms of the flow rate against the external force can be clearly observed at the low temperature $T = 0.1\varepsilon$. On the other hand, as the temperature increases, "jamming" region disappears even in the small external force and this "jamming" phenomena are likely related to the gas-liquid transition of the 2D LJ phase diagram. In the fundamental diagram, the change in the fluctuation in the metastable region is often discussed, whereas we cannot observe any fluctuation peak in our model. These results likely relate to the lack of the metastable branch and thus the flow rate may be represented by a single curve in our fundamental diagram. We also investigated the WCA molecular flow to extract the role of the attractive forces and found that attractive forces at the low temperature are dominant for the "jamming" phenomena.

The extension of this model to other transport models is straightforward. As

examples, grand canonical molecular simulations have been developed to examine the molecular transport by introducing explicit chemical potential gradients into the system.^{39),40)}

As emphasized in the introduction, we study a very simple model of the pipe with a bottleneck, while our model qualitatively shows the important features of the molecular transport through the bottleneck and is of importance for the architecture and functionality in the emerging field of nanomaterial systems.

Acknowledgements

The authors thank Hirofumi Wada for fruitful suggestions and Glenn Paquette for correcting proofs. The numerical calculations were carried out on Altix3700 BX2 at YITP of Kyoto University and this work was supported by the Grant-in-Aid for the Global COE Program "The Next Generation of Physics, Spun from Universality and Emergence" from the Ministry of Education, Culture, Sports, Science and Technology (MEXT) of Japan. This work is also supported by Grants-in-Aid of MEXT(Grant Nos. 21015016 and 21540384)

References

- 1) T. L. Pennec, K. J. Måløy, A. Hansen, M. Ammi, D. Bideau and X. Wu, Phys. Rev. E **53** (1996), 2257.
- 2) E. Longhi, N. Easwar and N. Menon, Phys. Rev. Lett. **89** (2002), 045501.
- 3) D. Helbing, Rev. Mod. Phys. **73** (2001), 1067.
- 4) T. Nagatani, Rep. Prog. Phys. **65** (2002), 1331.
- 5) S. Yamamoto, Y. Hieida and S. Tadaki, J. Phys. Soc. Jpn. **75** (2006), 114601.
- 6) T. Kretz, A. Grünebohm and M. Schreckenberg, J. Stat. Mech. **10** (2006), P10014.
- 7) M. Isobe, D. Helbing and T. Nagatani, Phys. Rev. E **69** (2004), 066132.
- 8) R. Nagai, M. Fukamachi and T. Nagatani, Physica A **367** (2006), 449.
- 9) A. Carminati, A. Kaestner, H. Fhler, P. Lehmann, D. Or, E. Lehmann and M. Stampioni, Phys. Rev. E **76** (2007), 026311.
- 10) P. Burriel, J. Claret, J. Ignés-Mullol and F. Sagués, Phys. Rev. Lett. **100** (2008), 134503.
- 11) H. W. Liepmann and A. Roshko, *Elements of Gas Dynamics* (Wiley, New York, 1957).
- 12) S. Sreenivasan, R. Cohen, E. López, Z. Toroczkai and H. E. Stanley, Phys. Rev. E **75** (2007), 036105.
- 13) D A. Doyle et al., Science **280** (1998), 69.
- 14) D. J. Bonhuis, J. Zhang, B. Hornblower, J. Mathé, B. I. Shklovskii and A. Meller, Phys. Rev. Lett. **97** (2006), 128104.
- 15) J. Zhang, A. Kamenev and B. I. Shklovskii, Phys. Rev. Lett. **95** (2005), 148101.
- 16) D. Wallacher, N. Künzner, D. Kovalev, N. Knorr and K. Knorr, Phys. Rev. Lett. **92** (2004), 195704.
- 17) A. Berezhkovskii and G. Hummer, Phys. Rev. Lett. **89** (2002), 064503
- 18) S. Gruener and P. Huber, Phys. Rev. Lett. **100** (2008), 064502
- 19) T. H. Nishino and H. Hayakawa, J. Phys. Soc. Jpn. **74** (2005), 2655
- 20) C. König, M. Fonin, M. Laufenberg, A. Biehler, W. Bühner, M. Kläui, U. Rüdiger and G. Güntherodt, Phys. Rev. B **75** (2007), 144428
- 21) H. Tanigawa, A. Yamaguchi, S. Kasai and T. Ono, J. Appl. Phys. **99** (2006), 08G520.
- 22) T. Koyama, G. Yamada, H. Tanigawa, S. Kasai, N. Ohshima, S. Fukami, N. Ishiwata, Y. Nakatani and T. Ono, Appl. Phys. Express. **1** (2008), 101303.
- 23) A. Himeno, S. Kasai and T. Ono, Appl. Phys. Lett. **87** (2005), 243108.
- 24) K. To, Phys. Rev. E **71** (2005), 060301.
- 25) S. Hörnlück, M. v. Hecke and P. Dimon, Phys. Rev. E **67** (2003), 021304.
- 26) D. Helbing and A. Johansson, Phys. Rev. Lett. **97** (2006), 168001.

- 27) V. Vargiamidis and H. Polatoglou, *Phys. Rev. B* **71** (2005), 075301
- 28) S. Midgley and J. B. Wang, *Phys. Rev. B* **64** (2001), 153304
- 29) K. Koga, G. T. Gao, H. Tanaka and X. C. Zeng, *Nature* **412** (2001), 802.
- 30) G. Hummer, J. C. Rasaiah and J. P. Noworyta, *Nature* **414** (2001), 188.
- 31) P. Pierobon, M. Mobilia, R. Kouyos and E. Frey, *Phys. Rev. E* **74** (2006), 031906.
- 32) P. Greulich and A. Schadschneider, *J. Stat. Mech.* **4** (2008), P04009.
- 33) V. Popkov and G. M. Schütz, *Europhys Lett.* **48** (1999), 257.
- 34) O. G. Jepps, S. K. Bhatia and D. J. Searles, *Phys. Rev. Lett.* **91** (2003), 126102.
- 35) Y. Tajima and T. Nagatani, *Physica A* **291** (2001), 545.
- 36) T. Nagatani, *Physica A* **300** (2001), 558.
- 37) C. T. Veje and P. Dimon, *Phys. Rev. E* **56** (1997), 4376.
- 38) B. Smit and D. Frenkel, *J. Chem. Phys.* **94** (1991), 5663.
- 39) R. F. Cracknell, D. Nicholson and N. Quirke, *Phys. Rev. Lett.* **74** (1995), 2463.
- 40) G. S. Heffelfinger and F. v. Swol, *J. Chem. Phys.* **100** (1994), 7548.